Journal of Power Sources 196 (2011) 7030–7034

Contents lists available at ScienceDirect

Journal of Power Sources

journal homepage: www.elsevier.com/locate/jpowsour

Short communication

Sulfur-graphene composite for rechargeable lithium batteries

Jia-Zhao Wang[a,b,*], Lin Lu[a], Mohammad Choucair[c], John A. Stride[c,d], Xun Xu[a], Hua-Kun Liu[a,b]

[a] Institute for Superconducting and Electronic Materials, University of Wollongong, NSW 2522, Australia
[b] ARC Centre of Excellence for Electromaterials Science, University of Wollongong, NSW 2522, Australia
[c] School of Chemistry, University of New South Wales, Sydney 2052, Australia
[d] Bragg Institute, Australian Nuclear Science and Technology Organisation, PMB 1, Australia

ARTICLE INFO

Article history:
Received 12 August 2010
Received in revised form
28 September 2010
Accepted 29 September 2010
Available online 7 October 2010

Keywords:
Sulfur-graphene composite
Lithium battery
Charge/discharge
Capacity

ABSTRACT

Sulfur-graphene (S-GNS) composites have been synthesized by heating a mixture of graphene nanosheets and elemental sulfur. According to field emission electron microscopy, scanning electron microscopy with energy dispersive X-ray mapping, Raman spectroscopy, and thermogravimetric analysis, sulfur particles were uniformly coated onto the surface of the graphene nanosheets. The electrochemical results show that the sulfur-graphene nanosheet composite significantly improved the electrical conductivity, the capacity, and the cycle stability in a lithium cell compared with the bare sulfur electrode.

1. Introduction

Over the past decade, substantial efforts have been devoted to developing energy storage systems that can be coupled to renewable sources, including wind, wave, and solar energy, as well as regenerative braking from vehicular transport, as a fundamental solution to our serious emission and pollution problems. Among the various types of rechargeable batteries, the lithium/sulfur battery system is a very attractive candidate, because at 1672 mA h g^{-1} and 2600 W h kg^{-1}, respectively, elemental sulfur has almost the highest theoretical capacity and highest theoretical power density of all known cathodes. In addition to the high capacity, utilization of sulfur as a cathode material has the advantages of natural abundance, low cost, and environmental friendliness.

However, the development of lithium sulfur-based batteries has met several challenges, such as (i) sulfur is highly electrically insulating [1], which leads to poor electrochemical accessibility and low utilization of the sulfur in the electrode; (ii) polysulfide, which forms during the first discharge step of a sulfur/metal battery, is generally soluble in conventional organic solvent based electrolyte, which causes the rapid irreversible loss of sulfur active materials over repeated cycles. To successfully operate the lithium-sulfur battery, the sulfur cathode material must be well combined with a conductive additive and a strong adsorbent agent [2–7]. Various carbon materials have been intensively investigated as additives for Li/S batteries, such as mesoporous carbon [4], active carbon [8], and carbon nanotube [9]. However, these sulfur carbon composites still suffer extensive capacity fading.

In recent years, graphene, a one-atom-thick planar sheet of sp^2-bonded carbon atoms densely packed in a honeycomb crystal lattice, has attracted appreciable attention for use as an energy storage material, because of its superior electrical conductivity, high surface area of over 2600 m^2 g^{-1}, chemical tolerance, and broad electrochemical window [10]. It has been reported that graphene can be used as a carbon matrix to improve conductivity of electrode materials for lithium-ion batteries [10–16]. Herein, we synthesized sulfur-coated graphene composites and investigated graphene nanosheets as a carbon matrix to improve the performance of sulfur cathodes for rechargeable lithium batteries for the first time. Because of its good electrical conductivity [10,13], graphene in the composites acted as an electronic conductor.

2. Experimental

2.1. Materials synthesis

Highly porous graphene nanosheets (GNS) were synthesized via the solvothermal method, as reported previously [10], and then the GNS was mixed with elemental sulfur S in the weight ratio of 1:1.5, with the mixture designated S-GNS. The mixture was held at

* Corresponding author at: Institute for Superconducting and Electronic Materials, University of Wollongong, AIIM Facility, Innovation Campus, Squires Way, Fairy Meadow, NSW 2519, Australia. Tel.: +61 2 4298 1478; fax: +61 2 42215731.
E-mail address: jiazhao@uow.edu.au (J.-Z. Wang).

0378-7753/$ – see front matter © 2010 Elsevier B.V. All rights reserved.
doi:10.1016/j.jpowsour.2010.09.106

200 °C for 6 h to allow the melted elemental sulfur to infiltrate into the layer of graphene. Then, the temperature was increased to and held at 300 °C for 3 h, so that the vaporized sulfur was coated onto the graphene.

2.2. Materials characterization

The products were characterized using X-ray diffraction (XRD, GBC MMA) with Cu Kα radiation. The morphology and energy dispersive spectroscopy (EDS) mapping of the samples were obtained with a field-emission scanning electron microscopy (FESEM; JEOL 7500, 15 kV) and a JEOL JSM 6460A scanning electron microscope (SEM), respectively. Raman spectroscopy was conducted to further confirm that the as-prepared powders of S-GNS had been successfully produced, using a JOBIN YVON HR800 Confocal Raman system with 632.8 nm diode laser excitation on a 300 lines mm^{-1} grating at room temperature. Thermogravimetric analysis (TGA) was performed via a SETARAM Thermogravimetric Analyzer (France) in air to determine the changes in sample weight with increasing temperature and to estimate the amount of sulfur in the sample.

2.3. Electrochemical measurements

The S-GNS composite cathode slurry was made by mixing 80 wt.% composite with 10 wt.% carbon black and 10 wt.% polyvinylidene fluoride (PVDF) binder in N-methyl-2-pyrrolidinone (NMP) solvent. Sulfur cathode slurry containing 50 wt.% sulfur powder, 40 wt.% carbon black, and 10 wt.% PVDF binder was also prepared in the same way as described previously to compare with the S-GNS composite. The slurries were spread onto aluminum foil substrates. The coated electrodes were dried in a vacuum oven at 100 °C for 24 h and then pressed. Subsequently, the electrodes were cut to a 1 cm × 1 cm size. Homemade Teflon cells were assembled in an Ar-filled glove box. A conventional organic solvent electrolyte of 1 mol L^{-1} lithium bistrifluoromethanesulfonamide (LiTFSI) in poly(ethylene glycol) dimethyl ether 500 (PEGDME 500) was used. The cells were galvanostatically discharged and charged in the range of 1.5–3.0 V at a current density of 50 mA g^{-1}.

3. Results and discussion

3.1. Physical properties of substrates

Fig. 1(a) presents XRD patterns for the elemental sulfur and sulfur-graphene composite. The sulfur exists in a crystalline state. There are no clear characteristic peaks of sulfur for the sulfur-graphene composite. This indicates that embedded sulfur exists in fine particles and a highly dispersed state, with the crystalline sulfur most likely converted to amorphous sulfur by the heat treatment [17]. When the mixture of sulfur and graphene was thermally treated at 200 °C, sulfur would be expected to melt and coat the graphene nanosheets. At the higher temperature of 300 °C, sulfur existing on the external surface of the graphene nanosheets was sublimed. At the same time, sulfur gas could also diffuse into the pores of graphene. Fig. 1(b) presents the Raman spectrum of S-GNS composite powder. The Raman spectrum of the sulfur-graphene composite displays three peaks under 500 cm^{-1}, which are due to the sulfur particles [18], and another two peaks at around 1355 cm^{-1} and 1597 cm^{-1}, which are identified as the D band and the G band of graphene nanosheets [12]. This indicates that the sulfur-graphene composite was successfully synthesized using the physical vapor deposition method.

To investigate the morphology of the products, field emission scanning electron microscope (FESEM) images and scanning electron microscope (SEM) images were collected for GNS and S-GNS composite, and bare S, respectively. Fig. 2(a) shows that the bare S powder consists of microsized particles. Visualization of the pristine GNS by FESEM (Fig. 2(b)) shows well-packed layers of flakes composed of curved nanosheets with highly developed porous structure. After heat treatment of the mixture of S and GNS, the microsized S particles were melted and covered the graphene nanosheets (Fig. 2(c)). To verify that the sulfur was uniformly coated on the graphene, EDS mapping analysis was carried on the S-GNS composite (see Fig. 3). The bright spots correspond to the presence of the elements S and C, respectively, and indicate that S and C are distributed uniformly throughout the whole area.

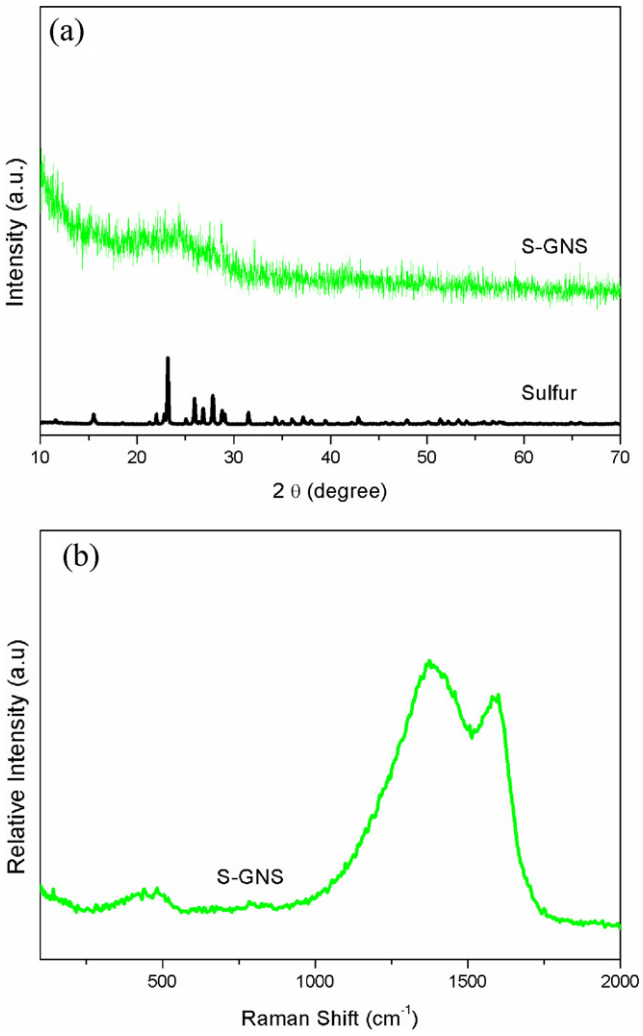

Fig. 1. (a) X-ray diffraction patterns for bare S and S-GNS composite and (b) Raman spectrum of S-GNS composite.

For quantifying the amount of graphene in the S-GNS composites, TGA was carried out in air. The samples were heated from 100 °C to 600 °C at a rate of 5 °C min^{-1}. Fig. 4 shows the TGA curves of the S-GNS samples, along with those of pure graphene and bare S powder. As can be seen from Fig. 4, the bare sulfur powder was burned completely at around 325 °C, and pure graphene started to be oxidised at 350 °C. Therefore, for the sample of S-GNS composite, the sulfur was burned off at the first stage, followed by the oxidation of the graphene powder in the second stage for temperatures above 350 °C. For the S-GNS composite, the weight loss in the first stage was about 22 wt.%, which represents the amount of sulfur.

Cyclic voltammogram (CV) of S-GNS composite electrode is shown in Fig. 5(a). Two reduction peaks were observed, which were due to the multiple reaction mechanisms of sulfur with lithium.

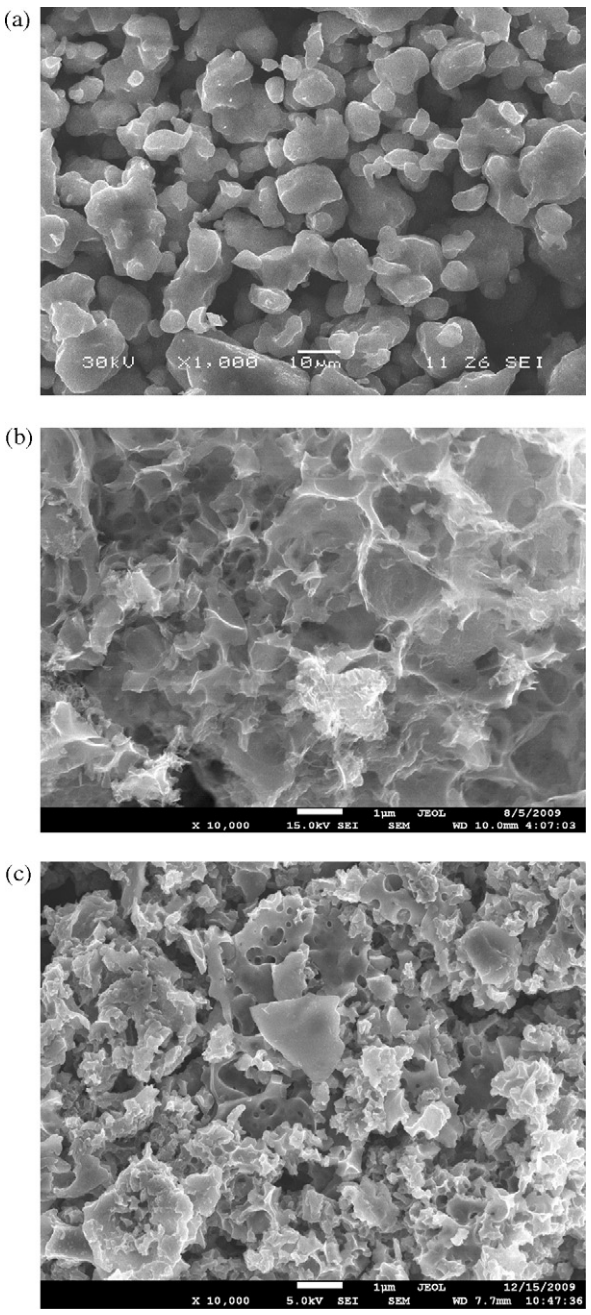

Fig. 2. (a) SEM image of bare S, (b) FE-SEM images of GNS and (c) S-GNS composite.

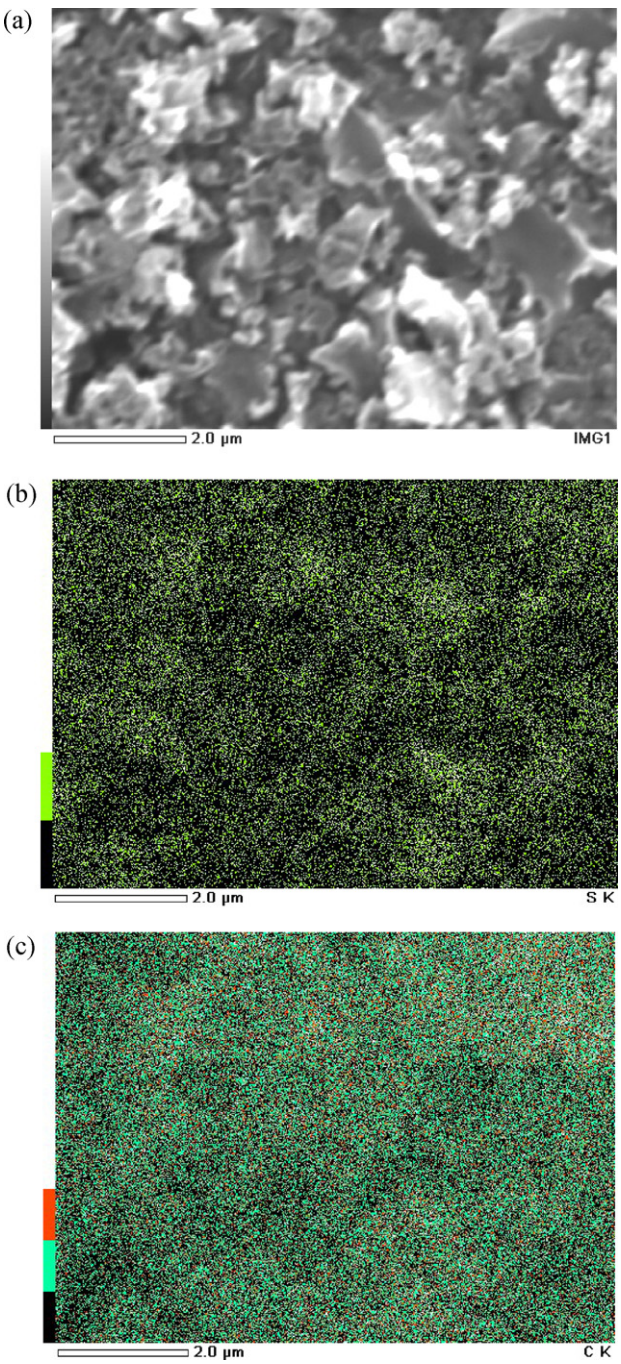

Fig. 3. SEM image obtained from S-GNS with corresponding EDS mapping for S and C.

It is proposed that the first step is the transformation of sulfur to lithium polysulfide at higher potential (Eq. (1)), and the second step is the change of lithium polysulfide to lithium sulfide (Li_2S) at lower potential (Eq. (2)) [19,20].

$$2Li + nS \rightarrow Li_2S_n \quad (n > 4) \tag{1}$$

$$2(n-1)Li + Li_2S_n \rightarrow nLi_2S \tag{2}$$

Since graphene in the composite is electrochemically inert in the potential region used, the (CV) redox peaks are only attributable to the oxidation and reduction of elemental sulfur, so therefore, no additional peaks were found for the S-GSN composite in comparison with pure S electrode [4].

According to the CV performance, it appears that all the redox processes took place in the range between 1.5 V and 3.0 V (versus Li/Li^+). Therefore, the potential range of 1.5–3.0 V (versus Li/Li^+) was selected for the continuous charge–discharge cycling process. Fig. 5(b) presents typical charge–discharge curves of S-GNS electrode in a rechargeable lithium cell. The charge–discharge curve shows two typical plateaus, which could be assigned to the two-step reaction of sulfur with lithium during the discharge process, as demonstrated in the CV measurement.

Fig. 6 shows discharge capacity versus cycle number for cells made with the S and S-GNS electrodes. The S-GNS electrode contains 17.6 wt.% sulfur. It was found that the initial discharge capacities of S and S-GNS composite are 1100 and 1611 mA h g^{-1}, respectively, at a current density of 50 mA g^{-1}. The initial capacity of the S-GNS electrode is higher than that of the pure sulfur electrode. Furthermore, the cycling stability of the sulfur graphene

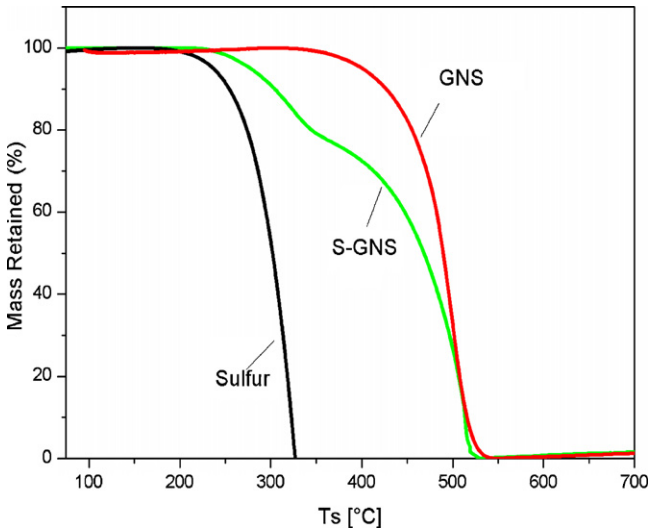

Fig. 4. Thermogravimetric analysis (TGA) curves of bare S, S-GNS composite and pure GNS.

composite is also improved. The improvement in the capacity and cycling stability of the cell with the S-GNS composite electrode may be because the graphene in the composite can improve the conductivity of the electrode.

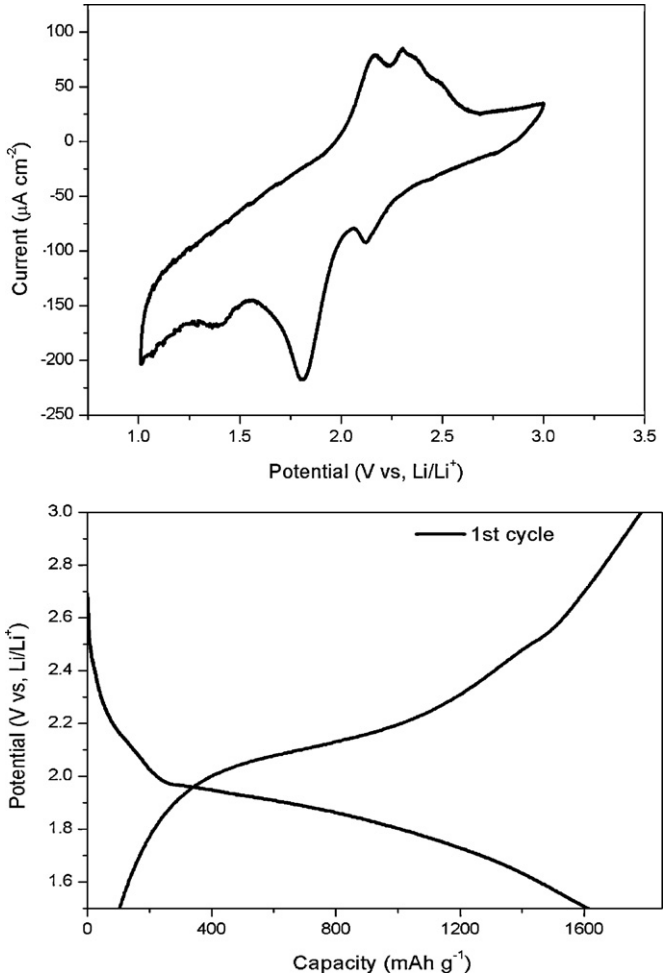

Fig. 5. (a) Cyclic voltammogram of S-GNS composite electrode and (b) charge–discharge curves of S-GNS composite.

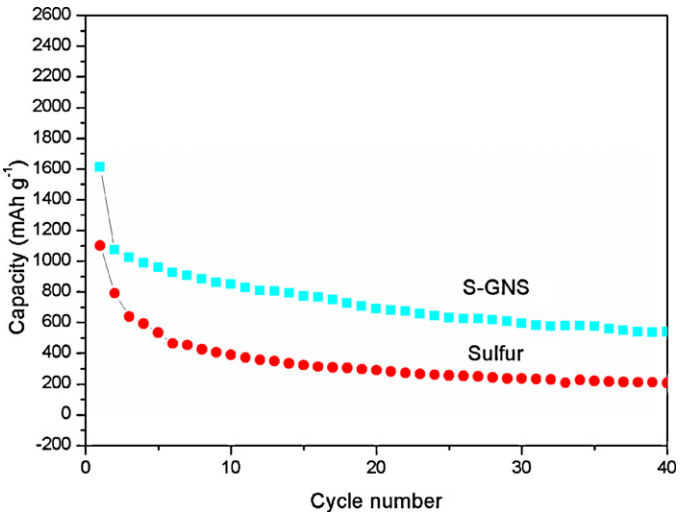

Fig. 6. Discharge capacities versus cycle number for the S-GNS composite and pure S electrodes.

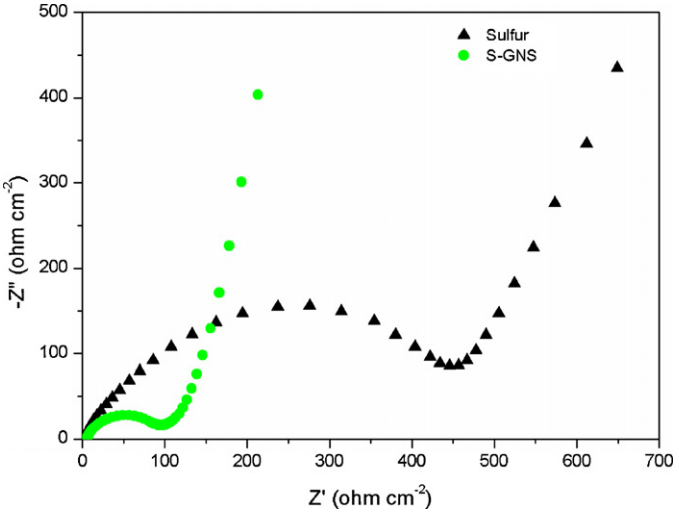

Fig. 7. Impedance plots for electrodes of bare S and S-GNS composite.

In order to verify that the graphene is responsible for the good performance of the cell with the S-GNS electrode, electrochemical impedance spectroscopy (EIS) measurements were performed on the pure S and S-GNS electrodes after 1 cycle (Fig. 7). At high frequencies, the impedance response exhibits a semicircular loop. The diameter of this semicircle gives the charge-transfer resistance, which is a measure of the charge transfer kinetics. The results show that the charge-transfer resistance of the cell with S-GNS electrode is lower than for the cell made from pure S electrode. This indicates that the novel composite of sulfur with graphene can improve the electrochemical kinetics of the sulfur in rechargeable lithium batteries [18].

4. Conclusion

Novel sulfur–graphene (S-GNS) composites were synthesized by heating a mixture of elemental sulfur and synthesized graphene nanosheets. The S-GNS composite shows a significantly improved capacity and cycle life compared to the bare S electrode. The materials utilization of sulfur is 96.35%.

Acknowledgements

Financial support provided by an Australian Research Council (ARC) Linkage Project (LP100100802) and an ARC Discovery Project (DP 0987805) are gratefully acknowledged. Many thanks also go to Dr. T. Silver for critical reading of the manuscript.

References

[1] J.A. Dean, Lange's Handbook of Chemistry, 3rd ed., McGraw-Hill, New York, 1985, pp. 3–5.
[2] X. Ji, K.T. Lee, L.F. Nazar, Nat. Mater. 8 (2009) 500–506.
[3] C. Liang, N.J. Dudney, J.Y. Howe, Chem. Mater. 21 (2009) 4724.
[4] J.Z. Wang, S.Y. Chew, Z.W. Zhao, S. Ashraf, D. Wexler, J. Chen, S.H. Ng, S.L. Chou, H.K. Liu, Carbon 46 (2008) 229–235.
[5] J.L. Wang, J. Yang, J.Y. Xie, N.X. Xu, Adv. Funct. Mater. 13 (2003) 6.
[6] M. Sun, S. Zhang, T. Jiang, L. Zhang, J. Yu, Electrochem. Commun. 10 (2008) 1819–1822.
[7] X. Yu, J. Xie, J. Yang, H. Huang, K. Wang, Z. Wen, J. Electroanal. Chem. 573 (2004) 121–128.
[8] J.L. Wang, J. Yang, J.Y. Xie, N.X. Xu, Y. Li, Electrochem. Commun. 4 (6) (2002) 499.
[9] L. Yuan, H. Yuan, X. Qiu, L. Chen, W. Zhu, J. Power Sources 189 (2009) 1141–1146.
[10] M. Choucair, P. Thordarson, J.A. Stride, Nat. Nanotechnol. 4 (2009), 30.
[11] M.D. Stoller, S. Park, Y. Zhu, J. An, R.S. Ruoff, Nano Lett. 8 (2008) 3498–3502.
[12] M. Yoshikawa, G. Katagiri, H. Ishida, A. Ishitani, Solid State Commun. 66 (11) (1988) 1177–1180.
[13] W. Choi, I. Lahiri, R. Seelaboyin, Y.S. Kang, Crit. Rev. Solid State Mater. Sci. 35 (2010) 52–71.
[14] D. Wang, R. Kou, D. Choi, Z. Yang, Z. Nie, J. Li, L.V. Saraf, J. Zhang, G.L. Graff, J. Liu, M.A. Pope, I.A. Aksay, ACS Nano 4 (3) (2010) 1587–1595.
[15] D. Wang, D. Choi, J. Li, Z. Yang, Z. Nie, R. Kou, D. Hu, C. Wang, L.V. Saraf, J. Zhang, I.A. Aksay, J. Liu, ACS Nano 3 (4) (2009) 907–914.
[16] J.K. Lee, K.B. Smith, C.M. Hayner, H.H. Kung, Chem. Commun. 46 (2010) 2025–2027.
[17] C. Lai, X.P. Gao, B. Zhang, T.Y. Yan, Z. Zhou, J. Phys. Chem. C 113 (2009) 4712–4716.
[18] J. Wang, J. Chen, K. Konstantinov, L. Zhao, S.H. Ng, G.X. Wang, Z.P. Guo, H.K. Liu, Electrochim. Acta 51 (2006) 4634–4638.
[19] H.S. Ryu, Z. Guo, H.J. Ahn, G.B. Cho, H. Liu, J. Power Sources 189 (2009) 1179–1183.
[20] H. Yamin, J. Penciner, A. Gorenshtain, M. Elam, E. Peled, J. Power Sources 14 (1985) 129.